Journal of Photochemistry and Photobiology A: Chemistry 207 (2009) 197–203

Contents lists available at ScienceDirect

Journal of Photochemistry and Photobiology A: Chemistry

journal homepage: www.elsevier.com/locate/jphotochem

Photocatalytic degradation using tungsten-modified TiO_2 and visible light: Kinetic and mechanistic effects using multiple catalyst doping strategies

Timothy Hathway, Erin M. Rockafellow, Youn-Chul Oh, William S. Jenks*

Department of Chemistry, Iowa State University, Ames, IA 50011-3111, USA

ARTICLE INFO

Article history:
Received 1 January 2009
Received in revised form 2 June 2009
Accepted 8 July 2009
Available online 16 July 2009

Keywords:
Tungsten
Titanium dioxide
Photocatalysis
Visible

ABSTRACT

Tungsten-modified titanium dioxide catalysts prepared from sol–gel methods and obtained commercially were compared for their photocatalytic activity using mechanistic probes designed to examine chemical pathways of oxidation. No special visible absorbance was noted for the sol–gel catalysts. However, an increase in the single-electron transfer chemistry with the presence of WO_x was noted, and a distinct wavelength dependence on the product ratios.

© 2009 Elsevier B.V. All rights reserved.

1. Introduction

Titanium dioxide is an excellent photocatalyst for the degradation of organic contaminants in water and air. Most organic compounds are degraded to CO_2, H_2O, and appropriate inorganic ions on exposure to TiO_2 in the presence of light and oxygen [1–7]. A distinct hindrance, however, for more widespread application of TiO_2 as a catalyst for removal of organic pollutants is its lack of absorption in the visible spectrum, as betrayed by its appearance as a white powder. Another is its relatively low efficiency. Modification of TiO_2 is thus an active and important field of research.

Of the three common phases of crystalline TiO_2, it is widely held that anatase (band gap = 3.2 eV, absorption $\leq$385 nm) is the most photocatalytically active, yet rutile (band gap = 3.0 eV, absorption $\leq$410 nm) absorbs light to the red of the anatase band edge. This poses an obvious advantage, when considering the utility of solar light, but still does not extend far into the visible, where the majority terrestrial solar energy lies. The most commonly used and most effective TiO_2 photocatalyst is probably DeGussa's P25, which contains adjoining anatase and rutile microcrystalline regions. Gray has shown that this extended functionality is due in large part to the extended near-visible absorption of the rutile phase, followed by rapid electron transfer between the phases, leading to enhanced charge separation and reduced energy wastage by electron–hole recombination [8,9].

In this sense, DeGussa P25 and other mixed-phase TiO_2 samples are inherently multi-component catalysts, but other multi-component strategies for enhancing photocatalysts have emerged as well [10,11]. One approach to building multi-component catalysts to increase physical charge separation and/or visible light absorption include nanodeposits of noble metal pools on the exterior of TiO_2 particles [12–15]. Another, more in the spirit of P25, is the overt use of additional semiconductors, such as CdS or WO_3, coupled to TiO_2 [16–20]. Kamat has outlined both core–shell and coupled geometries [16,17], but for practical purposes, we are concerned with the coupled case, which may be envisioned as small adjoining nanodomains. Here, both photogenerated holes and electrons are potentially accessible at the particle surface.

In this paper, we examine the photocatalytic chemistry of a series of WO_3-modified titanium dioxide samples [21–24]. The band gap of bulk WO_3 is 2.5 eV, which corresponds to absorption out to approximately 500 nm, well into the visible. Moreover, because of the absolute positions of the bands, conduction bond electrons from TiO_2 can migrate to WO_3, while the complementary migration can occur for valence band holes. With small percentages of tungsten, relative to titanium, it is also possible that simple substitutional doping may occur, with less predictable results.

A key issue, however, is whether the ordinary modes of reactivity for TiO_2 are maintained, enhanced, or destroyed [25]. We and others have generally drawn a distinction between hydroxyl-like ($HO^{\bullet}_{ads}$) and SET-initiated chemistry. (See, for example, Ref. [26].) Bahnemann has referred to these phenomenologically different reactivities as deriving from "deeply" and "surface" trapped holes, respectively [27]. Others, as summarized by Fujishima et al. [7], argue that the hydroxyl-like chemistry can occur away from the

* Corresponding author.
E-mail address: wsjenks@iastate.edu (W.S. Jenks).

1010-6030/$ – see front matter © 2009 Elsevier B.V. All rights reserved.
doi:10.1016/j.jphotochem.2009.07.010

particle surface, indicative of a diffusible intermediate (presumably HO• itself). Regardless of the claims of true action-at-a-distance, we have argued that SET chemistry has a more stringent requirement for pre-adsorption to the catalyst and shown this to be the case for both oxidative and reductive SET reactions [26,28].

In principle, if reactivity in WO_x-modified TiO_2 derives from the oxidative reactivity of holes residing in TiO_2 alone (surface or "deep"), then both the typical hydroxyl-like and single-electron transfer initiated chemistry ought still occur, assuming the reactivity is still dominated by adsorption on TiO_2 sites. The valence band for bulk WO_3 is at a higher potential than for TiO_2, which could result in hole trapping concentrated on these sites, which might, in turn, be observable in the oxidative behavior. There is also a possibility of true wavelength dependence of the chemistry because of the dopant, depending on the dynamics of hole trapping vs. substrate oxidation. However, if isolated WO_x sites are dilute within the TiO_2 matrix, the effects are harder to predict.

There are multiple methods of making WO_x-modified TiO_2, including an incipient wetness method, in which TiO_2 is at least partially coated with WO_x from solution deposition, and sol–gel methods, in which the tungsten is coprecipitated with the titanium and is presumably distributed throughout the catalyst. (We will use the term WO_x–TiO_2 below to mean tungsten-modified TiO_2 in the most general sense, and will be more precise when referring to specific preparations.)

We examine the oxidative chemistry of two sets of catalysts. First, we compare two commercial catalysts: PC50 and DT52 from Millenium chemicals. The latter of these is derived by treatment of the former to coat it with WO_x by an incipient wetness method, such as that described by Do et al. [21]. This process presumably results in segregated regions of WO_x on the TiO_2 particle. A second series is a set of sol–gel-prepared WO_x–TiO_2 catalysts with 0–5% tungsten, prepared according to the method of Li et al. [23]. By contrast, there is no evidence to suggest anything but a randomly formed mixed oxide for these materials. Rather than evaluate the chemistry by disappearance of a dye such as methylene blue [29], we use chemical probes originally proposed by Ranchella et al. [30] and Pichat and co-workers [31,32] that provide more detailed information regarding the chemical mechanisms of oxidation of these catalysts, revealing pathways through product analysis.

2. Experimental

2.1. General materials

1-*p*-Anisylneopentanol (**AN**) and the oxidized products of its degradation were synthesized and characterized as published previously [25]. Quinoline and its major oxidized products were obtained from Aldrich. Distilled water was purified from a Millipore MilliQ UV system and had a resistivity of $\geq$18 MΩ cm^{-1}. Commercial titania samples were PC50 and DT52 obtained from Millennium Chemical.

2.2. Preparation of WO_x–TiO_2 catalysts

WO_x–TiO_2 was prepared by a sol–gel method based closely on that of Li et al. [23]. A TiO_2 transparent sol was prepared by combining 17.5 g Ti(O-*n*Bu)$_4$, 120 mL ethanol, 15 mL acetic acid, and 5 mL de-ionized water. The mixture was aged for 1 day, stirring at room temperature. To this sol was added dropwise added 60 mL of aqueous solution of containing 4.56 g of ammonium paratungstate ($(NH_4)_{10}W_{12}O_{41}$, F.W. = 3042.55) under vigorous stirring over 2 h until WO_x–TiO_2 (3 mol% WO_x to TiO_2) gel is formed. Similarly, 0%, 1%, and 5% WO_x–TiO_2 samples were prepared by using appropriate amounts of ammonium paratungstate. Ammonium tungstate was also used in the same way to prepare a 3% WO_x–TiO_2 gel with a different W source; no detectable difference was found between materials made from the two precursors.

The WO_x–TiO_2 gels were aged 2 days with vigorous stirring, then 1 day undisturbed followed by 1 more day with vigorous stirring. The WO_x–TiO_2 gels were then dried with a rotary evaporator at 358 K. As the gels dried, they shrunk and coated the surface of their flasks, eventually forming powders. After drying, the samples were ground for 8 min in an agate ball mill.

Sintering was then carried out in porcelain crucibles. The furnace was heated at a moderate rate (10 K/min) to ensure that ejection of the volatiles did not discharge powder from the crucibles. The furnace was allowed to reach 923 K, which then stayed constant for 2 h. A calibrated thermocouple was placed in the center of the cluster of crucibles to continuously monitor the temperature at the location of the samples. The furnace was then allowed to cool down over the course of 2 h. The cooled powders were immediately transferred to storage vials.

2.3. Catalyst characterization

Powder X-ray diffraction (XRD) measurements were carried out at room temperature using a diffractometer with Cu Kα radiation. An accelerating voltage of 40 kV and an emission current of 30 mA were used.

X-ray photoelectron spectroscopy (XPS) was performed with a multi-technique spectrometer employing monochromatized Al Kα radiation. The instrumental Gaussian full-width at half maximum (GFWHM), which characterizes the resolution, was 0.65 eV for the Al source. The take-off angle was fixed at 45° and the X-ray source was run at 14 kV and 250 W. The emitted photoelectrons were sampled from a 1 mm^2 area. The XPS energy scale was calibrated against Au 4f$_{7/2}$ and Ag 3d$_{5/2}$ peaks at 84.0 and 368.27 eV, respectively. The sample was mounted on an indium foil for XPS analysis and placed in the XPS chamber, whose base pressure was about 3×10^{-10} Torr. Temperature was measured with a Type K thermocouple.

Particles were examined by scanning electron microscopy (SEM) using a variable pressure scanning electron microscope with 20 kV accelerating voltage and ~0.5 nA of beam current for imaging in 25 mm working distance. SEM-EDX analyses were performed to check for segregation of the tungsten. A high-purity Ge light-element X-ray detector was employed and the take-off angle was fixed at 30°.

2.4. Suspensions and photolyses

Photocatalytic degradations were carried out as described previously [25,33]. Broadly emitting fluorescent lamps centered at 419 nm (roughly 390–500 nm total range) or 350 nm (roughly 320–380 nm) were used. The spectral distributions are available in the supporting information. Ferrioxalate actinometry was employed in order to compare the rates between UV and visible reactions [34,35]. Initial conditions were 300 μM **AN** or 150 μM **Q** in water containing 1 g/L catalyst and all solutions were purged with O_2. The pH was controlled throughout the kinetic run reactions by careful addition of aqueous NaOH as necessary. The reported initial degradation rates were normalized for total lamp flux by means of potassium ferrioxalate actinometry.

3. Results

3.1. Catalyst characterization

Based on SEM analysis, the average particle size of the sintered, tungstated catalysts was in the range of 100 nm to 3 μm, which is much larger than P25 particles (Fig. 1d). Ball-milling was

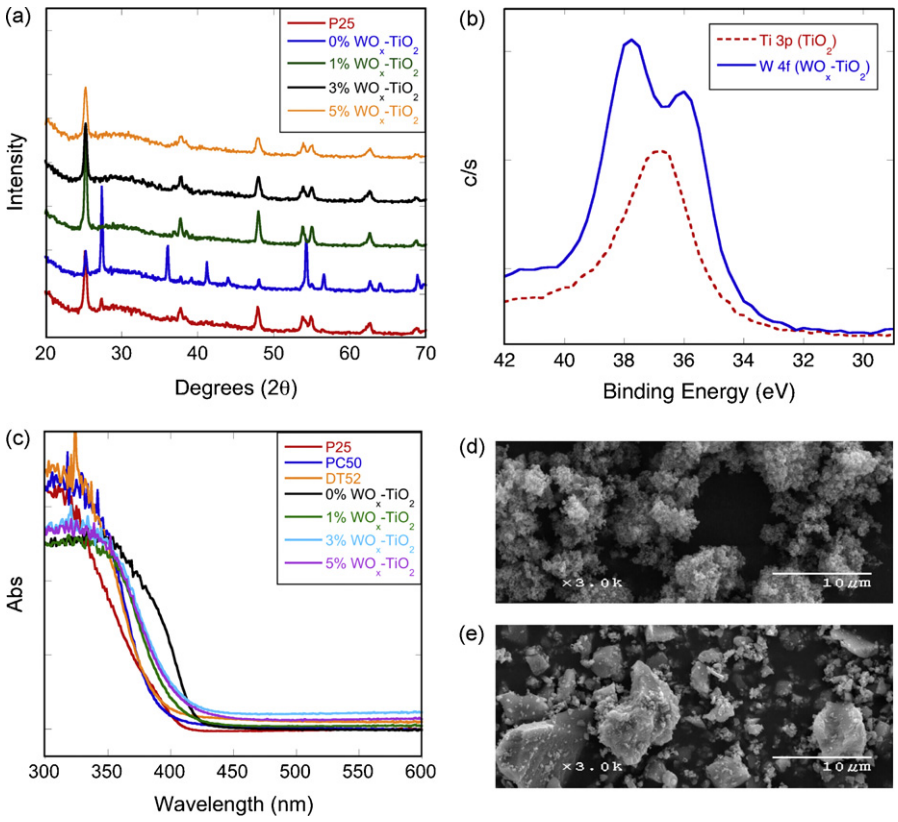

Fig. 1. Characterization of sol–gel catalysts. (a) Powder XRD patterns; (b) detail of XP spectrum of 3% WO_x–TiO_2; (c) diffuse reflectance UV–vis spectra; (d and e) SEM images of P25 (d) and 5% WO_x–TiO_2 after milling (e) on the same scale.

used to successfully grind the particles into the 20 nm regime (Fig. 2e), yielding both smaller particles and a tighter distribution of sizes.

As was noted by Li et al. [23], addition of WO_x to the sol–gel preparation of TiO_2 inhibited the conversion of anatase to rutile on annealing at 923 K. Studies of similar substitutionally W-doped titania catalysts show that W^{6+} exists in distorted octahedra. These cause long-range distortions that lead to anatase being favored over rutile up to temperatures higher than for undoped catalysts [36].

Fig. 1a shows the powder XRD of P25 (anatase and rutile), the undoped catalyst (0% WO_x–TiO_2, mainly rutile), and the doped materials (mainly anatase). Using the Scherrer equation, average crystallite sizes were found to be 15 nm, 18 nm, 23 nm, 28 nm, and

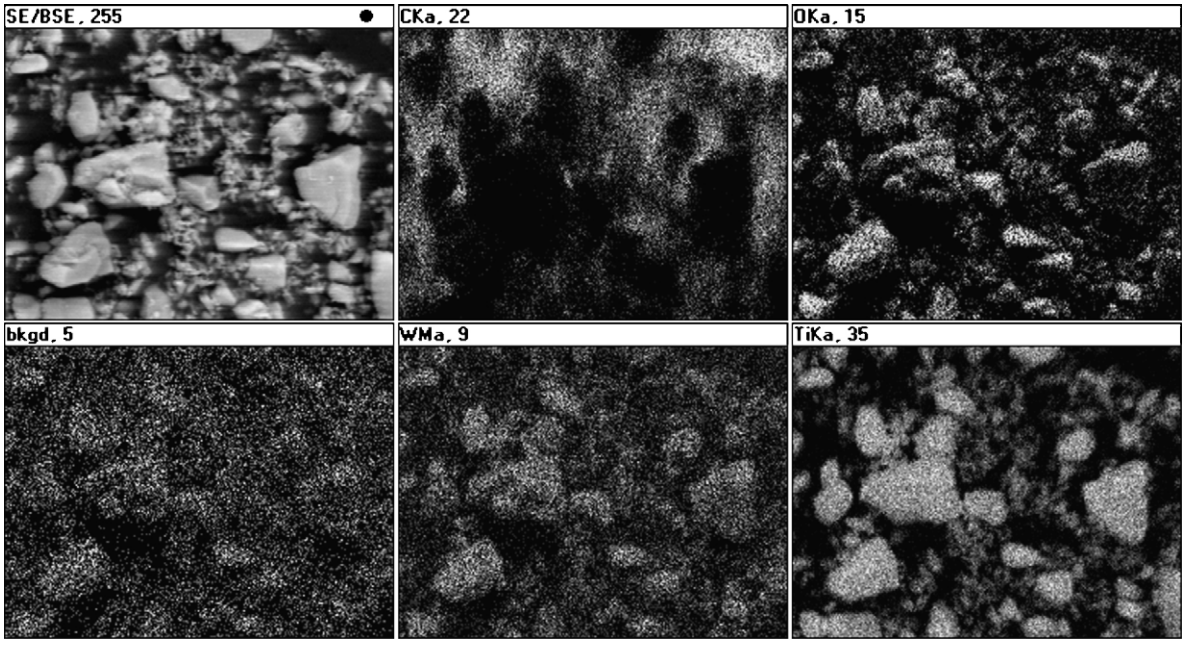

Fig. 2. SEM-EDX images of the 3% WO_x catalyst on the same scale as Fig. 1d and e. Clockwise from the top left: overall SEM, C signal, O signal, background, W signal, Ti signal.

19 nm for 5% WO_x, 3% WO_x, 1% WO_x, 0% WO_x, and DeGussa P25, respectively.

XPS was used to determine the oxidation state of W near the surface of the catalysts. Fig. 2b shows the underlying Ti 3p signal at 36.6 eV for the undoped sample. For the 3% WO_x–TiO_2 sample, the signal for the W^{6+} $4f_{7/2}$–$4f_{5/2}$ doublet at 36.0 eV is an inherently stronger peak and dominates the spectrum, with the apparent loss of resolution between the double peaks being due to the underlying Ti signal. Small contributions of other states are possible due to broad peaks [37]. Data from the XPS were also used to confirm the overall doping percentage (1.87% W, 32.80% Ti, remainder O, corresponding to 3 mol% W, relative to Ti, in TiO_2).

Diffuse reflectance UV–visible spectrophotometry (Fig. 2c) shows that there was not a dramatic shift in the absorption spectra of the catalysts outside of what is predictable from the XRD data. P25 shows the typical band edge of TiO_2, with a slight tail into the red due to rutile. DT52 and the PC50 from which it is made had nearly identical spectra. The most red-shifted absorption came from the 0% WO_xTiO_2. However, this effect can be attributed entirely to the great fraction of rutile in this material. We do not know why these materials exhibit a different result than the materials reported by Li et al. [23].

SEM-EDX was used to check for segregation of WO_3. The data in Fig. 2 shows an even distribution of W in the 3% W catalyst, though the resolution of the images (ca. 0.2 μm) is not good enough to demonstrate whether there are nano-sized aggregations on the TiO_2 particles, or whether the W is homogeneously dispersed on the atomic scale. The same results were obtained for the 1% and 5% WO_x catalysts. More SEM and SEM-EDX data are available in the Supporting Information.

3.2. Probe degradations

Because one of the important questions of modified photocatalysts is whether they are more functional with visible light than undoped TiO_2, the experiments described below were carried out with lamps whose irradiation is centered at 419 nm, to the red of the onset of absorption of the bare catalysts as documented in Fig. 1. This light source rests on the edge of the range separating near UV and visible light, but clearly enough, there is more light of this range available from ambient sunlight (the ideal light source) than the more commonly used true UV wavelengths. The irradiation frequencies of this lamp, however, are such that a small amount of light below 380 nm is available. As noted, other irradiations used lamps centered at 350 nm. No irradiations were done using light sources well into the visible (e.g., 500 nm and longer) because the catalysts do not directly absorb any light in these regions.

Initially, 4-methoxyresorcinol (2,4-dihydroxyanisole), was chosen as a probe because it exhibits a mixture of SET and hydroxyl chemistry with P25 and the PC series of catalysts [25,26]. However, initial experiments using 420 nm irradiation indicated a high degradation efficiency. Subsequent preliminary experiments using a white light source and a 435 nm high pass cutoff filter suggested that any differences between the catalysts were being overwhelmed by visible-light mediated degradation that could be attributed to the formation of a charge transfer complex between this very electron rich arene and TiO_2, analogous to the reports of Agrios et al. [38,39]. We therefore resorted to the less electron rich probes shown in Scheme 1.

3.2.1. Kinetic traces

The initial degradative steps of probe molecules quinoline (**Q**) and 1-*p*-anisylneopentanol (**AN**) have been discussed at length previously [25,30,31]; the essentials are illustrated in Scheme 1 and can be summarized by noting the differing products predominant for single-electron transfer (SET) chemistry and hydroxyl-type chemistry. These two probes were chosen for their lack of strong adsorption to the TiO_2 and for their well-defined partial degradation chemistry. Conditions were chosen on the basis of previous work [25] under which both SET and hydroxyl products would normally be observed.

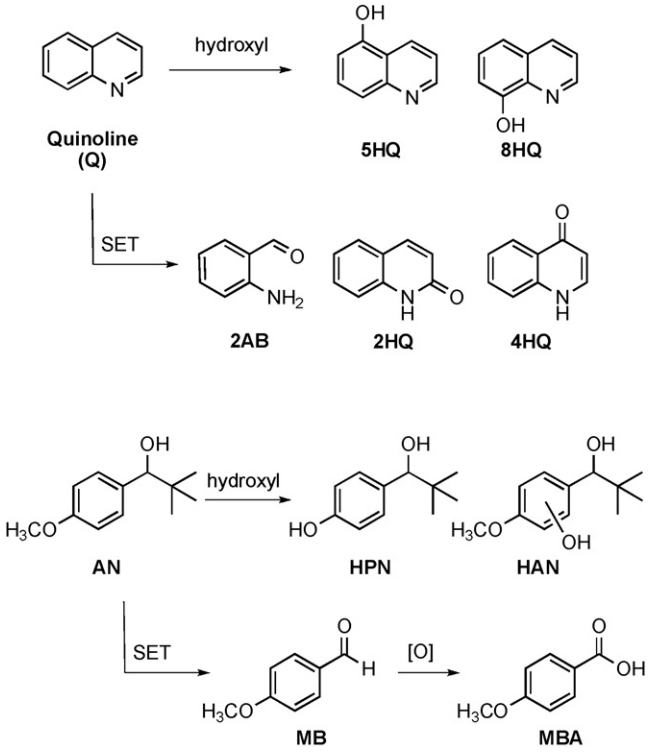

Scheme 1.

Kinetic traces were obtained. As seen in Fig. 3, which illustrates the data obtained at 419 nm, the traces could be acceptably fit to zero order decays for degradation of up to approximately 25%. The results are given numerically in Table 1, and the values were reproducible within a 5% standard deviation. Immediately striking is the two order of magnitude increase in rate at 350 nm, relative to 419 nm.

For **AN**, the clearly superior catalyst is DT52, with the others varying without a discernable pattern. The rate of degradation of quinoline is not especially pH sensitive, despite its pK_a being between 4.5 and 5, such that the protonated and deprotonated forms are predominant at pH 3 and 6, respectively. Adsorption is difficult to measure quantitatively, but it is expected that quinolinium, due to its greater water solubility and positive charge, would be less adsorbed to the catalyst, which is also positively charged at pH 3. At pH 6, adsorption of quinoline through the nitrogen lone pair is expected. The rate of degradation does not vary much, however, suggesting that adsorption to the catalyst is not rate-determining for this compound.

3.2.2. Product studies

The sole product obtained for low conversion of **AN** with the 419 nm bulbs was *p*-methoxybenzoic acid (**MBA**). This is clearly the result of a two-step oxidation whose initial product is *p*-methoxybenzaldehyde (**MB**). The second oxidation step may be photochemical or a result of the formation of hydrogen peroxide and either autoxidation or Bayer-Villager chemistry. In any case, it is clear that **MB** is oxidized more rapidly than it is formed and thus does not accumulate. For the 5% WO_x–TiO_2 catalyst, both the usual **MBA** and hydroxylated products (Scheme 1) were observed,

Table 1
Degradation rates of **AN** and **Q** with various catalysts.

Catalyst	Rate (μM/min)[a]					
	AN pH 2 420 nm	**Q** pH 3 420 nm	**Q** pH 6 420 nm	**AN** pH 2 350 nm	**Q** pH 3 350 nm	**Q** pH 6 350 nm
PC50	2.00	1.52	1.91	354	154	287
3% DT52	6.70	5.45	6.99		597	616
0% WO_x–TiO_2	3.20					
1% WO_x–TiO_2	0.90					
3% WO_x–TiO_2	0.63	3.27	2.10		145	329
5% WO_x–TiO_2	1.27	7.09	5.75	179	605	228

[a] All rages were reproducible to standard deviations of ≤5%.

though the total accumulated intensity of the products was only about 10% of that of the other catalysts. The simplest explanation for the lower accumulation of intermediates is that they are degraded faster than they are formed, implying that the 5% WO_x–TiO_2 catalyst was superior from this perspective.

The 350 nm bulbs were also used to determine product ratios under UV irradiation. In distinct contrast to the 419 nm irradiations, all four products (**MB**, **MBA**, **HPN**, and **HAN**) were found in very comparable amounts for low conversion.

For degradation of **Q**, both $HO^{\bullet}_{ads}$-type products (**5HQ** and **8HQ**) and SET products (**2AB**, **2HQ**, and **4HQ**) are observed on 419 nm irradiation. At low pH, where quinoline is protonated, the hydroxyl type products predominate, whereas the SET products are found at higher concentration at pH 6. The ratios of initially formed (SET products)/($HO^{\bullet}_{ads}$-type products) are given in Table 2. With 350 nm irradiation at pH 3, the hydroxyl products still predominate; at pH 6, the dominance of SET products declines, relative to the 419 nm values.

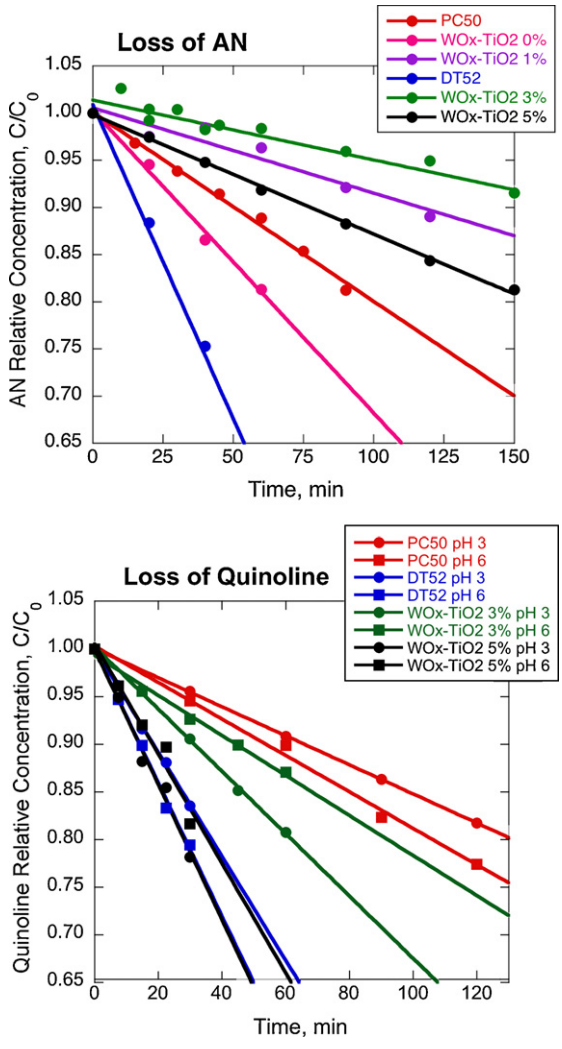

Fig. 3. Kinetic traces for degradation of **AN** (pH 2) and **Q** (pH 3 or 6) by various photocatalysts using irradiation centered at 419 nm.

Table 2
Ratio of initial SET products to hydroxyl-type products[a] in quinoline degradations.

Catalyst	pH 3 420 nm	pH 6 420 nm	pH 3 350 nm	pH 6 350 nm
PC50	0.08	9.5	0.11	0.63
3% DT52	0.54	11	0.13	1.2
3% WO_x–TiO_2	0.15	15	0.43	4.3
5% WO_x–TiO_2	0.25	4.2	<0.01	0.89

[a] See Scheme 1.

4. Discussion

In keeping with other publications examining the efficacy of tungstated titanium dioxide catalysts, we find DT52, the tungsten-treated PC50 derivative is more active than its parent material. The same cannot be directly concluded for the sol–gel samples examined here, because the crystal composition of the undoped sol–gel sample is a qualitatively different mix of anatase and rutile nanodomains than the others, as demonstrated in Fig. 1a. From this point of view, it appears that incipient wetness tungsten-coating of otherwise optimized TiO_2 photocatalysts may be an important empirical parameter for use in achieving the most active catalyst possible. Empirically, we are unaware of any evidence suggesting that the presumably homogeneous distribution of WO_x throughout the particle by the sol–gel (or other related) methods presents any special advantage in photocatalytic degradations besides stabilizing the anatase crystal structure (the more active titania polymorph) at high temperatures during catalyst preparation.

Two causes for increased reactivity of WO_x-modified TiO_2 have been proposed: the ability of the WO_3 to trap electrons (and thus preserve holes), and an increase of surface acidity, which is thought to improve the binding of Lewis bases [40]. There is not a consistent pattern of rates among the sol–gel prepared samples, but there is a consistent increase in both rate and proportion of SET products, comparing DT52 to PC50. This latter result suggests that enhanced surface binding may be important.

The materials we prepared (and DT52) do not have extensive absorption into the visible. Nonetheless, the 419 nm lamps we used overemphasize irradiation at the very red edge; only a modest percentage of the lamps' output is below 400 nm, and very little below 380 nm. The two order of magnitude change in rates of photolysis comparing 350–419 nm bulbs is at least in very large part due to the much smaller absorption of light by our catalysts in the latter case, since the actinometer counts all of the photons, absorbed by catalyst or not.

In our previously published work [25], partial degradation of **AN** with PC50 (or related catalysts) and 350 nm irradiation at pH 2 yielded a product mixture containing similar amounts of SET and $HO^{\bullet}_{ads}$ products. The present data, with the tungstated catalysts, give the same result. However, we find that only the electron transfer products are observed when irradiating at the red edge of the absorption band, with one exception (5% WO_x–TiO_2). A much smaller total sum of products and some hydroxyl chemistry was observed for the 5% WO_x–TiO. This result is probably due to more efficient degradation of **MBA** by 5% WO_x–TiO_2. The observation of a small amount of **HAB** and **HPN** is consistent with the idea that the **MB** and **MBA**, out-compete the **AN** for the specific adsorption locations that lead to SET reactivity (and get degraded in the process). However, it is not obvious why the phenomenon of the more efficient degradation of **MB** and **MBA** is limited to the 5% WO_x sample.

The red edge irradiation used with quinoline as a probe at pH 6 also shows a relative increase for SET products for every catalyst. At pH 3, the effect is less dramatic. In that the relative increase of SET chemistry at 419 nm is observed for PC50 and the undoped sol–gel TiO_2, it is clearly not a special feature due to the tungsten; rather it is an inherent feature of the interaction between the probes and TiO_2. The two simplest explanations are (1) there is a wavelength dependence on TiO_2 photocatalysis at the red edge of absorption that is generally unnoticed because it represents such a small portion of the excitation spectrum; (2) there is a charge-transfer band or other specific interaction between the small population of adsorbed probes and TiO_2 whose light absorption may extend further into the visible than the classic red edge of the catalyst absorption. Charge transfer interactions between arenes and TiO_2 are well documented in more functionalized cases [39,41]. We cannot be definitive here, but prefer the second explanation, given that the effect is much smaller for quinolinium ion at pH 3 than for the other two cases. Qunolinium's positively charged nature presumably inhibits binding to the positively charged TiO_2, and acts as a control – in combination with **AN** at pH 2 – for the effect being mitigated solely by the protonation state of the catalyst under acidic conditions.

5. Conclusions

The results reported here add to the literature that suggests that tungstated TiO_2 can be a catalyst that is functionally superior to its unmodified parent in terms of the speed of degradation for photocatalytic applications. No special advantage was found for sol–gel preparations that presumably disperse WO_x throughout the catalyst over comparable surface-modified species.

As documented by the diffuse reflectance spectra, surface coating of WO_x (e.g., DT52) does not have a significant effect on the light absorbed by the bare photocatalyst. Any effects on the absorption of the photocatalysts made by the sol–gel method may easily derive more from subtly different ratios of anatase and rutile in the annealed catalysts, since WO_x inhibits the conversion to rutile.

Product distributions for partial degradation are affected by the modification of the TiO_2. With surface modification (DT52 vs. PC50), the tendency was for the added tungsten to increase the fraction of SET-derived products, which accompanied an acceleration of overall reaction. This might be explained either by greater adsorption of the organic to the modified catalyst or by a longer lifetime of the SET-active "hole" before finding an alternative trap site that results in hydroxyl chemistry. Of these, the former, simpler explanation is more appealing, but more evidence would be required to be certain.

Also, a wavelength dependence was found. Irradiation at the red edge of TiO_2 absorption (and beyond) favored the cleavage reactions that have been attributed to SET chemistry for **AN** and the regiochemistry of hydroxylation that indicates SET chemistry for **Q**. In the absence of evidence to the contrary, the simplest explanation is a previously unknown charge transfer band formed on adsorption to the catalyst by almost any arene.

Acknowledgements

The authors thank the National Science Foundation (CHE 0518586) for financial support of this work. We are grateful to Clemens Burda for allowing us to obtain diffuse reflection spectra on his instrumentation. We also gratefully acknowledge the assistance of Jim Anderegg with the XPS data.

Appendix A. Supplementary data

Supplementary data associated with this article can be found, in the online version, at doi:10.1016/j.jphotochem.2009.07.010.

References

[1] P.K.J. Robertson, D.W. Bahnemann, J.M.C. Robertson, F. Wood, Handbook of Environmental Chemistry, vol. 2, Springer Verlag, 2005, pp. 367–423.
[2] D. Bahnemann, J. Cunningham, M.A. Fox, E. Pelizzetti, P. Pichat, N. Serpone, in: G.R. Helz, R.G. Zepp, D.G. Crosby (Eds.), Book, Photocatalytic Treatment of Waters, CRC Press, 1994, pp. 261–316.
[3] P. Pichat, Environ. Sci. Pollut. Control Series 26 (2003) 77–119.
[4] W.S. Jenks, in: V.H. Grassian (Ed.), Book, The Organic Chemistry of TiO_2 Photocatalysis of Aromatic Hydrocarbons, CRC Press, Boca Raton, 2005, pp. 307–346.
[5] D.F. Ollis, E. Pelizzettti, N. Serpone, in: N. Serpone, E. Pelizzetti (Eds.), Book, Heterogeneous Photocatalysis in the Environment: Application to Water Purification, John Wiley & Sons, New York, 1989, pp. 603–637.
[6] N. Serpone, E. Pelizzetti (Eds.), Photocatalysis: Fundamentals and Applications, John Wiley & Sons, New York, 1989.
[7] A. Fujishima, X. Zhang, D.A. Tryk, Surface Sci. Rep. 63 (2008) 515–582.
[8] D.C. Hurum, A.G. Agrios, K.A. Gray, T. Rajh, M.C. Thurnauer, J. Phys. Chem. B 107 (2003) 4545–4549.
[9] D.C. Hurum, K.A. Gray, J. Phys. Chem. B 109 (2005) 977–980.
[10] A.G. Agrios, P. Pichat, J. Appl. Electrochem. 35 (2005) 655–663.
[11] A.G. Agrios, K.A. Gray, in: V.H. Grassian (Ed.), Book, Beyond Photocatalytic Environmental Remediation: Novel TiO_2 Materials and Applications, Taylor and Francis, Boca Raton, 2005, pp. 369–390.
[12] I. Izumi, W.W. Dunn, K.O. Wilbourn, F.-R.F. Fan, A.J. Bard, J. Phys. Chem. 84 (1980) 3207–3210.
[13] Z. Goren, I. Willner, A.J. Nelson, A.J. Frank, J. Phys. Chem. 94 (1990) 3784–3790.
[14] Y.M. Gao, W. Lee, R. Trehan, R. Kershaw, K. Dwight, A. Wold, Mater. Res. Bull. 26 (1991) 1247–1254.
[15] J.M. Herrmann, J. Disdier, P. Pichat, A. Fernandez, A. Gonzalez-Elipe, G. Munuera, C. Leclercq, J. Catal. 132 (1991) 490–497.
[16] D. Liu, P. Kamat, J. Phys. Chem. 97 (1993) 10769–10773.
[17] C. Nasr, P.V. Kamat, S. Hotchandani, J. Electroanal. Chem. 420 (1997) 201–207.
[18] S. Hotchandani, P.V. Kamat, Chem. Phys. Lett. 191 (1992) 320–326.
[19] K. Vinodgopal, I. Bedja, P.V. Kamat, Chem. Mater. 8 (1996) 2180–2187.
[20] C. Nasr, S. Hotchandani, P.V. Kamat, Proc. Electrochem. Soc. 97–20 (1997) 130–140.
[21] Y.R. Do, W. Lee, K. Dwight, A. Wold, J. Solid State Chem. 108 (1994) 198–201.
[22] G. Ramis, G. Busca, C. Cristiani, L. Lietti, P. Forzatti, F. Bregani, Langmuir 8 (1992) 1744–1749.
[23] X.Z. Li, F.B. Li, C.L. Yang, W.K. Ge, J. Photochem. Photobiol. A 141 (2001) 209–217.
[24] J. Papp, S. Soled, K. Dwight, A. Wold, Chem. Mater. 6 (1994) 496–500.
[25] T. Hathway, W.S. Jenks, J. Photochem. Photobiol. A 200 (2008) 216–224.
[26] X. Li, J.W. Cubbage, W.S. Jenks, J. Photochem. Photobiol. A 143 (2001) 69–85.
[27] D. Bahnemann, in: P. Boule (Ed.), Book Photocatalytic Detoxification of Polluted Waters, vol. 2 L, Springer, Berlin, Germany, 1999, pp. 285–351.
[28] Y.-C. Oh, X. Li, J.W. Cubbage, S. Jenks William, Appl. Catal. B: Environ. 54 (2004) 105–114.
[29] X. Yan, T. Ohno, K. Nishijima, R. Abe, B. Ohtani, Chem. Phys. Lett. 429 (2006) 606–610.
[30] M. Ranchella, C. Rol, G.V. Sebastiani, J. Chem. Soc. Perkin Trans. 2 (2000) 311–315.
[31] L. Cermenati, P. Pichat, C. Guillard, A. Albini, J. Phys. Chem. B 101 (1997) 2650–2658.
[32] L. Cermenati, A. Albini, P. Pichat, C. Guillard, Res. Chem. Intermed. 26 (2000) 221–234.
[33] E.M. Rockafellow, X. Fang, B.G. Trewyn, K. Schmidt-Rohr, S. Jenks William, Chem. Mater. 21 (2009) 1187–1197.
[34] A.K. Chakraborti, L. Sharma, M.K. Nayak, J. Org. Chem. 67 (2002) 6406–6414.
[35] C.G. Hatchard, C.A. Parker, Proc. Royal. Soc. A 235 (1956) 518–536.

[36] M. Fernandez-Garcia, A. Martinez-Arias, A. Fuerte, J.C. Conesa, J. Phys. Chem. B 109 (2005) 6075–6083.
[37] J.F. Moulder, W.F. Stickle, P.E. Sobol, K.D. Bomben, Handbook of X-Ray Photoelectron Spectroscopy, Perkin-Elmer Corporation (Physical Electronics), Eden Prairie, MN, 1992.
[38] A.G. Agrios, K.A. Gray, E. Weitz, Langmuir 19 (2003) 5178.
[39] A.G. Agrios, K.A. Gray, E. Weitz, Langmuir 20 (2004) 5911–5917.
[40] K. Tennakone, O.A. Ileperuma, J.M.S. Bandara, W.C.B. Kiridena, Semicond. Sci. Technol. 7 (1992) 423–424.
[41] A.G. Agrios, K.A. Gray, E. Weitz, Langmuir 19 (2003) 1402–1409.